Analysis of Radiated Emissions From a Printed Circuit Board Using Expert System Algorithms

Yan Fu and Todd Hubing, *Fellow, IEEE*

***Abstract*—Three algorithms developed for expert system electromagnetic compatibility tools are used to evaluate a printed circuit board design. The maximum radiated emissions estimated by the algorithms are compared to the measured data for various board configurations. The algorithms identify the most important electromagnetic interference source mechanisms, drawing attention to the design parameters that have the most significant effect on the radiated emissions.**

***Index Terms*—Circuit board, common-mode, current driven, expert system, radiated EMI, voltage driven.**

I. Introduction

COMPUTER modeling software based on electromagnetic compatibility (EMC) expert system algorithms can be used to identify problems with a printed circuit board (PCB) layout before the first hardware is built. Unlike numerical electromagnetic (EM) modeling software (which solves for fields due to specific structures) or EMC design rule checkers (which look for layout features that violate selected design guidelines), expert system tools examine boards in much the same manner as a professional EMC engineer. They evaluate possible electromagnetic interference (EMI) sources, coupling paths, and antennas and then identify and rank potential EMC problems. An expert system provides assistance to the nonexpert by identifying potential problems and guiding the designer toward possible solutions. Expert systems are also useful tools for experienced EMC engineers, because they can process an enormous amount of information quickly, allowing human experts to focus their attention on the specific problems identified by the software [1]–[7].

Expert system algorithms to evaluate and identify EMC problems with PCB designs have been developed and are described in the literature [2], [3], [7]. These algorithms analyze PCB sources and structures to estimate the maximum likely radiated emissions due to a particular coupling mechanism. The purpose of these estimates is not to predict the results of an EMI test but rather to determine whether a particular feature of the board layout is likely to result in an EMI problem. This paper discusses three algorithms: the *voltage-driven common-mode radiation* algorithm, the *current-driven common-mode radiation* algorithm, and the *power bus radiation* algorithm. These algorithms were developed and validated in previous publications [7]–[12]. This paper applies these algorithms to the analysis of an actual PCB design. By loading or unloading the circuits on this board and by changing the position of an attached cable, the dominant emission source mechanisms are changed. These changes are predicted by the algorithms and verified by the measurements.

Manuscript received June 6, 2005; revised September 13, 2005.

Y. Fu is with the Department of Electrical and Computer Engineering, University of Missouri-Rolla, Rolla, MO 65409 USA (e-mail: yan_fu99@yahoo.com).

T. Hubing was with the Department of Electrical and Computer Engineering, University of Missouri-Rolla, Rolla, MO 65409 USA. He is now with Clemson University, Clemson, SC 29634 USA (e-mail: hubing@clemson.edu).

Digital Object Identifier 10.1109/TEMC.2007.888182

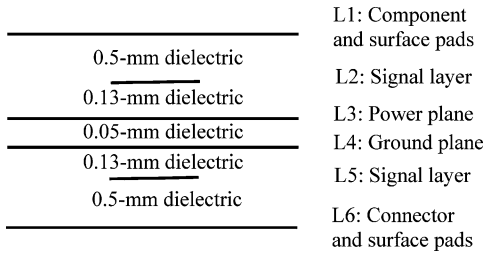

Fig. 1. Layer stack up of the test board.

II. Description of Test Boards

A multilayer test board was used to evaluate the expert system algorithms experimentally. This test board was previously developed for a study of the effects of layer spacing and dielectric materials on power bus noise [13]. Figs. 1 and 2 show the layer stackup and layout of the board.

The six-layer circuit board is 7.6 cm $\times$ 5.0 cm. Power and ground planes are located on layers 3 and 4 with a spacing of 0.05 mm. Signals are routed on layers 2 and 5. The components consist of one 50-MHz oscillator, one bulk decoupling capacitor, eight octal clock buffers, 28 load capacitors, and 32 local decoupling capacitors. A 50-MHz oscillator drives the input pins of one of the octal clock buffers (U7); the other buffers are driven by U7. A subminiature type A (SMA) coaxial connector was used to supply 3.3-V power to the board. The 1-Ω resistors were connected in series with the four power pins of one of the buffers, making it possible to measure the power currents to this buffer.

III. Expert System Analysis of the Test Board

A. Voltage-Driven Radiation Algorithm Result

1) Algorithm Description: The electric fields that couple directly to attached cables from a trace, heatsink, or other structure can induce common-mode currents on the cables, resulting in radiated emissions. This source mechanism is referred to as *voltage driven*, since the magnitude of the common-mode (CM) current is proportional to the signal voltage and is independent of the signal current [8]. Fig. 3 illustrates this voltage-driven mechanism. Assuming that the board is electrically small, the electric fields coupled to the attached cable can be represented by a capacitance between the trace and the cable $C_{t\text{-}c}$ [9].

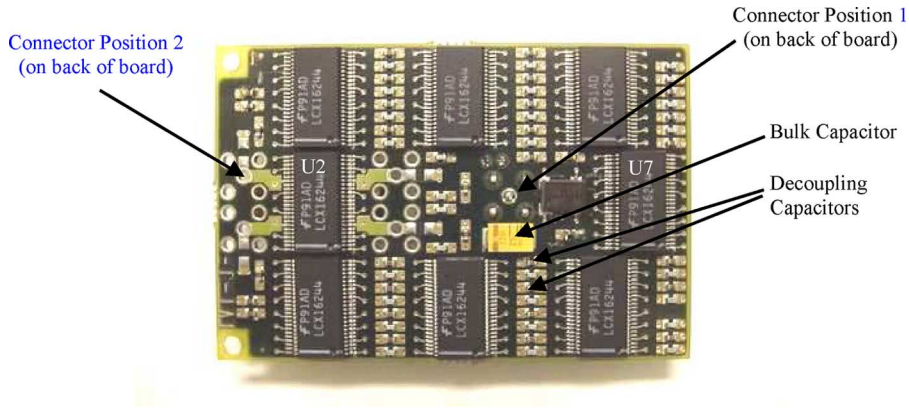

Fig. 2. Layout of the test board.

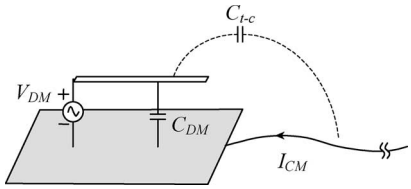

Fig. 3. Voltage-driven mechanism due to an attached cable.

If the length of the attached cable is much longer than the board dimensions, the radiated emissions are dominated by the CM current on the cable. Approximating the antenna as an isotropic source, the radiated power is given by

$$P_{\text{rad}} \approx \oint\!\!\oint \frac{1}{2}\frac{|E|^2}{\eta_0} ds = \frac{4\pi r^2 |E|^2}{2\eta_0} \equiv \frac{1}{2} I_{CM}^2 R_{\text{rad}} \tag{1}$$

where $\eta_0 = 120\pi$, and R_{rad} is the radiation resistance of the antenna. For a resonant dipole antenna, the worst-case radiation resistance is of the order of 100 Ω, so the maximum radiated field magnitude is approximately

$$|E| \approx \sqrt{30 R_{\text{rad}}}\frac{I_{CM}}{r} \approx (55\ \Omega)\frac{I_{CM}}{r}. \tag{2}$$

Since, in general, the radiated emissions are measured in a semianechoic chamber, the estimated field is multiplied by a factor of 2 to account for the worst-case reflection off the floor. The CM current can be expressed in terms of an equivalent CM voltage V_{CM} appearing between the board and the cable [8]. The maximum radiated field is then given by

$$|E|_{\max} \approx \frac{2V_{CM}}{r}\sqrt{\frac{30}{R_{\text{rad}}}} \approx 1.1\frac{V_{CM}}{r} \tag{3}$$

and the magnitude of the equivalent CM voltage source is

$$V_{CM} = \frac{C_{t-c}}{C_{\text{in}}} V_{DM} \tag{4}$$

where $C_{t\text{-}c}$ is the total capacitance between the trace and the attached cable, and C_{in} is the input capacitance of the wire antenna model, which is approximately given by [14]

$$C_{\text{in}} \approx C_{\text{board}} \approx 8\varepsilon_o \sqrt{\frac{\text{Board Area}}{\pi}} \tag{5}$$

where C_{board} is the estimated self-capacitance of the board.

In the general case, the total capacitance between a trace (or heatsink) and the attached cable $C_{t\text{-}c}$, is approximately [9]

$$C_t = \frac{6.189}{\pi}\frac{h_t}{W}\frac{C_{DM} l_t}{\ln\left[1 + 3.845\left(\frac{L}{W}\right)\right]} \quad \text{(for coupling to a trace)} \tag{6}$$

$$C_H = 4\pi\varepsilon_o \sqrt[3]{\text{Volume of heatsink}} \quad \text{(for coupling to a heatsink)} \tag{7}$$

where h_t is the height of the trace over the return plane, l_t is the length of the trace, and L and W are the length and width of the board, respectively. C_{DM} is the capacitance of the strip with an infinitely wide return plane, which is given by [15], [16]

$$C_{DM} = 2\pi\varepsilon_o \left\{\ln\left[\frac{F_1 \cdot h_t}{a} + \sqrt{1 + \left(\frac{2h_t}{a}\right)^2}\right]\right\}^{-1} \tag{8}$$

where a is the width of the trace, and F_1 is given by

$$F_1 = 6 + (2\pi - 6)\exp\left\{-\left(30.666\frac{h_t}{a}\right)^{0.7528}\right\}. \tag{9}$$

2) Board Analysis Using the Voltage-Driven Radiation Algorithm: The voltage-driven algorithm was first applied to the test board for the case where the buffers were not loaded. The CM voltage and the radiated electric field due to each signal trace were obtained from (4) and (3), respectively. The board parameters used to calculate the radiation and their values are listed in Table I.

Since the clock buffers were not loaded, there was little signal current. In this case, we would expect the voltage-driven emissions to be dominant. There were 28 buffer load mounting pads each with a size of about 2 mm × 1.5 mm (four for each buffer) on the top layer of the board. The pads were connected to the buffers through 28 traces, each with a length of about 1 cm and a width of about 0.5 mm, on the second signal layer of the board. Assuming all voltage signals are in phase, the total radiated field should be the sum of the contributions from each trace. Fig. 4 shows the envelope of the estimated worst-case radiation from the board at a distance of 3 m calculated using the

TABLE I
PARAMETERS NEEDED FOR VOLTAGE-DRIVEN ALGORITHM

Parameter	Description	Value
L	Board length	7.6 cm
W	Board width	5.0 cm
h_t	Trace height over power planes	0.625 mm for top layer traces 0.125 mm for second layer traces
l_t	Trace length	Depends on individual trace
a	Trace width	Depends on individual trace
t_r	Rise time of the voltage signal	1 ns
t_f	Fall time of the voltage signal	1 ns
T	Period of the signal	20 ns
τ	Pulse width of the signal	10 ns

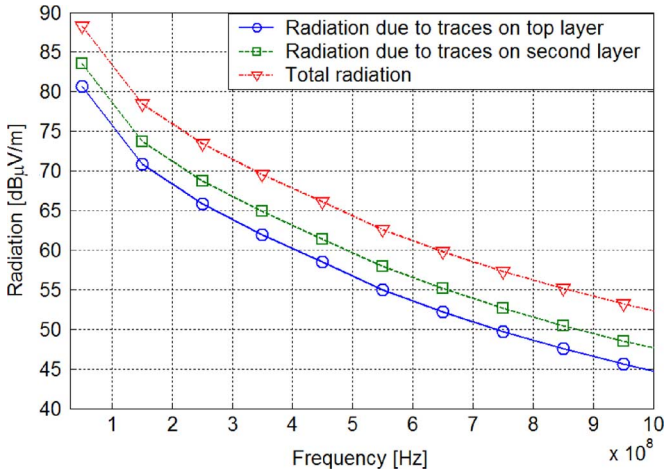

Fig. 4. Radiation from the board calculated using the voltage-driven radiation algorithm.

voltage-driven radiation algorithm. Note that the algorithm predicts that the radiated emissions from this board with an attached cable are capable of exceeding the Federal Communications Commission (FCC) or the International Special Committee on Radio Interference (CISPR) limits by many decibels, particularly below a few hundred megahertz.

B. Current-Driven Common Mode Radiation Algorithm Results

1) Algorithm Description: Since PCBs have a finite width, a portion of the magnetic fields due to the signal currents wraps around the board, and there is an effective voltage drop across the return plane. This voltage drop, in turn, can induce CM currents that drive various structures and cables on the board [10]. Fig. 5 illustrates the cable-to-board current-driven CM radiation mechanism. A CM voltage V_{CM} is induced by the differential-mode signal current I_{DM}. This CM voltage induces a CM mode current I_{CM} between the cable and the right half of the board.

The expert system estimates the CM voltage generated by a signal trace by approximating the branch inductance of the current path as [10]

$$L_p = \left(\frac{4}{\pi^2}\right)\frac{\mu_0 l_t h_t}{\text{dist1} + \text{dist2}} \tag{10}$$

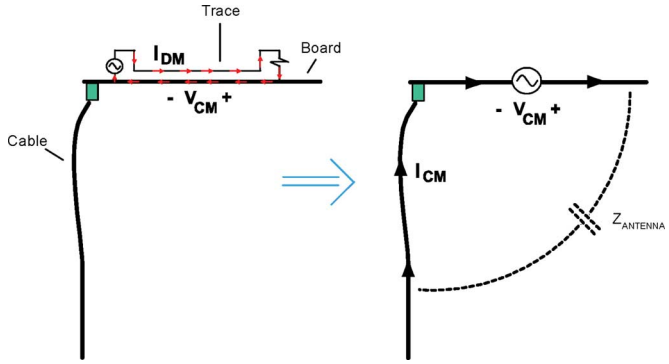

Fig. 5. Simple configuration illustrating current-driven common-mode radiation.

where h_t is the height of the trace over the return plane, and dist1 and dist2 are the two shortest distances to the boundary of the board from the center point of the trace segment. The potential difference due to each trace i is given by

$$V_{\text{ret},i} = \omega L_{p,i} I_{DM,i}. \tag{11}$$

The equation given in (11) shows that the impedance associated with the plane is proportional to the signal frequency. This relationship is valid when the trace is electrically short. However, this voltage will reach its maximum value and will no longer increase when the trace is no longer electrically short. This maximum value will always occur within a quarter wavelength of the load. Therefore, (11) is modified as

$$V_{\text{ret},i} = \begin{cases} \omega L_{p,i} I_{DM,i}, & \omega \le \frac{\pi c}{2 l_t \sqrt{\varepsilon_r}} \\ \frac{\pi c L_{p,i} I_{DM,i}}{2 l_t \sqrt{\varepsilon_r}}, & \omega > \frac{\pi c}{2 l_t \sqrt{\varepsilon_r}} \end{cases} \tag{12}$$

where c is the velocity of propagation in free space.

The expert system algorithms allow users to specify the characteristics of the signal current. However, by default, the current drawn from each device is assumed to have a triangular shape, as shown in Fig. 6.

The spectrum of the current on the signal traces is calculated as

$$I_{DM}(n) = \frac{2I_{p1}}{t_1}\frac{\sin^2(n\pi t_1/T)}{(n\pi t_1/T)^2} - (-1)^n \frac{2I_{p2}}{t_2}\frac{\sin^2(n\pi t_2/T)}{(n\pi t_2/T)^2}. \tag{13}$$

The total potential difference across the board is the sum of the contributions from each trace

$$V_{\text{ret}} = \sqrt{\sum V_{\text{ret},i}^2}. \tag{14}$$

When there is one cable attached to the board, the maximum radiated fields at a distance of 3 m due to the current-driven voltage between the cable and board is [7]

$$|E_{\text{cable-to-board}}| = 0.365\frac{100 V_{\text{ret}}}{\sqrt{100^2 + \frac{1}{(\omega C_B)^2}}} \tag{15}$$

where C_B is the absolute capacitance of the board in (5).

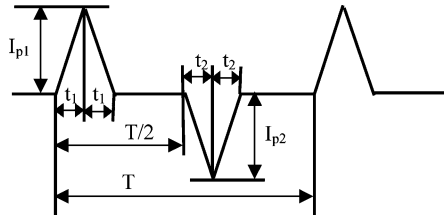

Fig. 6. Current waveform on signal traces.

TABLE II
PARAMETERS NEEDED FOR CURRENT-DRIVEN RADIATION ALGORITHM

Parameter	Description	Value
L	Board length	7.6 cm
W	Board width	5.0 cm
h_t	Height of trace above plane	Depends on individual trace
l_t	Trace length	Depends on individual trace
ε_r	Dielectric permittivity	3.88
dist1	Shortest distance to one board edge	Depends on individual trace
dist2	Shortest distance to another board edge	Depends on individual trace
Δt	Current pulse width	3 ns
T	Period of the signal	20 ns
C_L	Load capacitance of the signal traces	16 x 7 pF

2) Board Analysis Using the Current-Driven CM Radiation Algorithm: The algorithm was first applied to the test board when the buffers were not loaded. For the board under analysis, there were no heatsinks, and there was only one cable attached to the board. Therefore, only the cable-to-board radiation was evaluated. The parameters needed to calculate the radiation by the current-driven CM radiation algorithm and their values are listed in Table II.

There were a total of seven signal traces on the second layer of the board contributing to the current-driven CM radiation. One of the eight clock buffer ICs was driving the remaining seven clock buffer ICs. The signal current on each trace was approximated as a triangular pulse with a pulse width of Δt, a period of T, and a peak value of $I_p = C_L V_{CC}/\Delta t$. Fig. 7 shows the envelope of the maximum estimated radiated emissions calculated using the current-driven CM radiation algorithm. At low frequencies (e.g., below 300 MHz), the radiation is limited primarily by the ability of the board-cable structure to form an efficient antenna. At higher frequencies, the radiation falls off in proportion to the amount of energy in the source current waveform.

C. Power Bus Radiation Results

1) Algorithm Description: Transient currents drawn by the active devices on a PCB are a source of power bus noise. For high-speed digital systems, the resulting power bus voltage fluctuation cannot only lead to functional problems but also result in significant radiated emissions. The power bus radiation algorithm computes the radiation coming directly from the power bus on a board with power planes. The maximum intensity of the radiated emissions from a rectangular power bus structure can be derived, based on an analytical cavity-resonator model. The effect of components mounted on the board is modeled

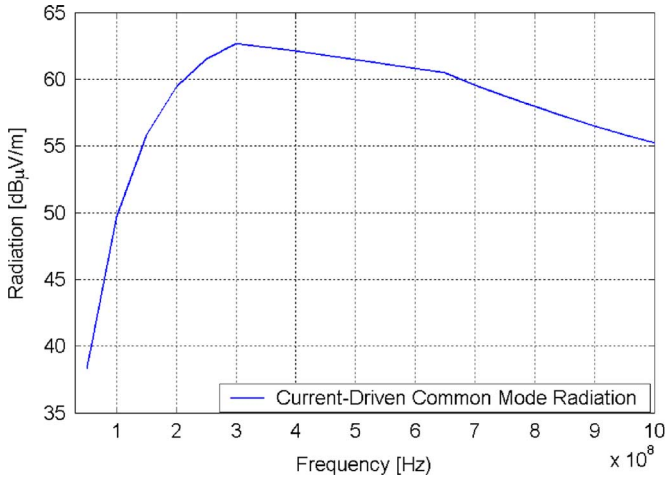

Fig. 7. Maximum emissions calculated using the current-driven CM radiation algorithm.

by modifying the propagation constant of the waves within the power bus structure. The maximum radiated field intensity is given by [17]

$$|E| = \frac{120I}{\varepsilon_r \min(L,W)} \frac{h}{r} Q(f) \tag{16}$$

where I is the current drawn from the power planes, L and W are the equivalent width and length of the power planes, h is the spacing between the plane pair, r is the distance from the board to the measurement point, and $Q(f)$ is the resonance quality factor of the power bus structure. $Q(f)$ is determined by the dielectric loss, conductive loss, and component loss of the power bus and is given by

$$Q(f) = \left(\frac{1}{Q_d} + \frac{1}{Q_c} + \frac{1}{Q_{\text{comp}}} \right)^{-1} \tag{17}$$

where Q_d, Q_c, and Q_{comp} are the quality factors of the power bus resonance due to dielectric loss, conductive loss, and component loss, respectively, and are given by

$$Q_d(f) = \frac{1}{\tan \delta} \tag{18}$$

$$Q_c = \frac{h}{\delta_s} \tag{19}$$

and [11], [12]

$$Q_{\text{comp}} = \frac{\omega C_0 \left(R_c^2 + \omega^2 L_c^2 \right)}{N_c R_c} \tag{20}$$

where $\tan \delta$ is the dielectric loss tangent, δ_s is the skin depth of the plane conductors, N_c is the number of components connected to the planes, C_0 is the interplane capacitance, R_c is the average resistance of the components (algorithm default $= 300\, m\Omega$), and L_c is the average connection inductance of the components.

The current drawn from the planes can be estimated, based on the current drawn by the active devices. For CMOS devices,

TABLE III
PARAMETERS NEEDED FOR POWER BUS RADIATION ALGORITHM

Parameter	Description	Value
L	Board length	7.6 cm
W	Board width	5.0 cm
h	Space between power planes	0.05 mm
ε_r	Dielectric permittivity	3.88
R_c	Average resistance of the components	0.3 ohms
L_c	Average inductance of the components	1.4 nH
t_1	Rise/fall time of the current signal	1.5 ns
t_2	Rise/fall time of the current signal	1.5 ns
T	Period of the signal	20 ns
C_{PD}	Power dissipation capacitance	20 pF/gate

the current (Fig. 6) drawn by each active device is estimated as

$$I_{p1} = \frac{(C_{PD} + C_L)\Delta V}{\Delta t} \tag{21}$$

$$I_{p2} = \frac{C_{PD}\Delta V}{\Delta t} \tag{22}$$

and

$$t_1 = t_2 = \frac{\Delta t}{2} \tag{23}$$

where C_{PD} is the power dissipation capacitance of the device, ΔV is the voltage change during the transition, Δt is the rise or fall time of the transition, and C_L is the load capacitance. The spectrum of the current can be calculated using (13).

The device draws current from the power planes and the decoupling capacitors. Only the current drawn from the power planes contributes to the power bus radiation. The fraction of the current drawn from the power planes is given by

$$p = 1 - \frac{M}{L_{\text{decap}}} \tag{24}$$

where M is the mutual inductance between the two vias associated with the decoupling capacitor and the power/ground pin, and L_{decap} is the parasitic self-inductance of the decoupling capacitor connection. M is calculated as [18]

$$M = \frac{\mu_0 h}{2\pi}\left[\ln\left(\frac{R}{s+r}\right) - 0.75\right] \tag{25}$$

where h is the dielectric thickness, s is the space between two vias, r is the radius of the via, and R is the equivalent radius of the board, which can be approximated as $(L+W)/4$.

The current drawn from the power planes is then given by

$$I = pI_{\text{device}}. \tag{26}$$

The expert system uses the most significant current drawn by one device to estimate the maximum radiation from the board due to power bus radiation.

2) Board Analysis Using the Power Bus Radiation Algorithm: The algorithm was first applied to the test board when the buffers were not loaded. The parameters needed to calculate the radiation by the power bus radiation algorithm and their values are listed in Table III.

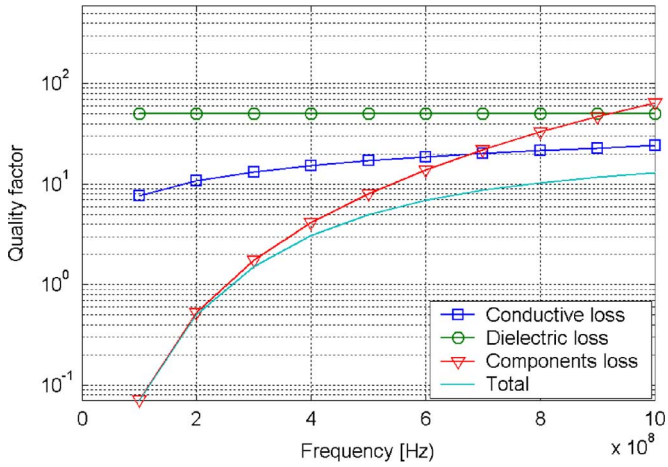

Fig. 8. Quality factor of the test board.

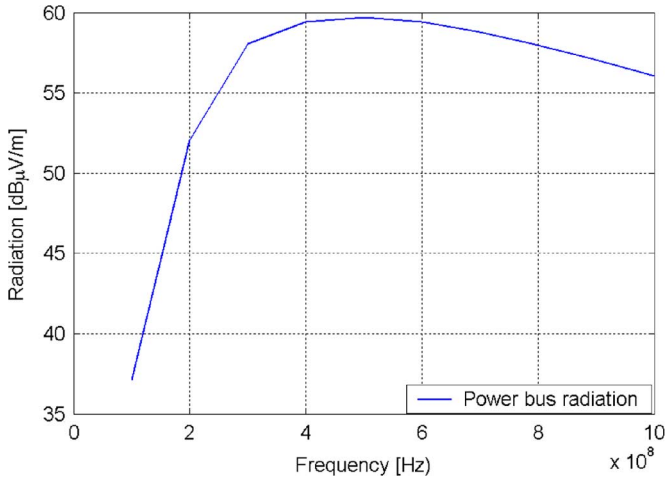

Fig. 9. Radiation from the board calculated using the power bus radiation algorithm.

Fig. 8 shows the calculated quality factors for the test board. The component loss dominates at frequencies approximately below 700 MHz. At higher frequencies, the conductive loss and dielectric loss begin to dominate, because the parasitic inductance of the components limits the current that can be drawn from them. Fig. 9 shows the maximum radiation from the board calculated by the power bus radiation algorithm. At low frequencies, the emissions are limited primarily by the component loss. Above 500 MHz, the radiation decreases primarily because the energy in the power bus current waveform decreases.

IV. MEASUREMENT OF NCMS TEST BOARDS

A. Measurement Setup

The radiation from the test board was measured in a semi-anechoic chamber. The board was powered by a power supply outside the chamber through a coaxial cable. The board was put on a turntable inside the chamber. A log-periodic antenna was located 3 m away to measure the radiation from the board. The antenna was connected to a spectrum analyzer located outside the chamber. The height of the antenna was scanned from 1 to 1.6 m in 10-cm increments. At each height, the turntable was

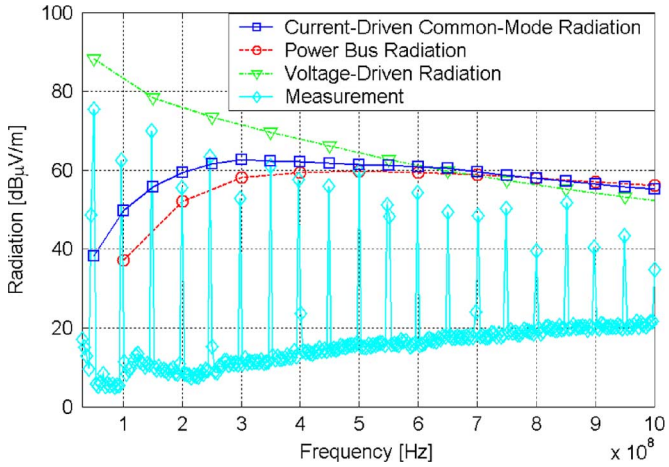

Fig. 10. Comparison of measured radiation and expert system algorithms calculation when the buffers were not loaded.

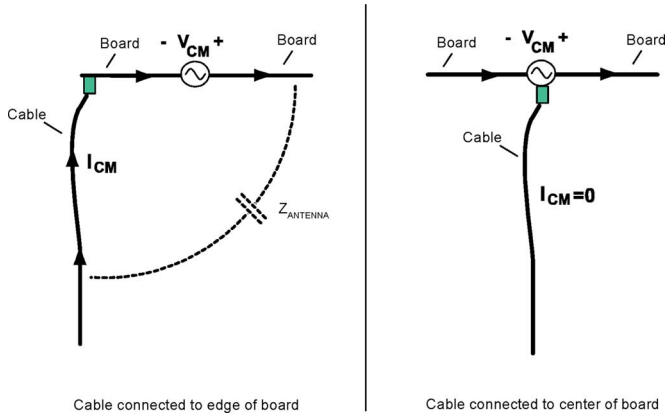

Fig. 11. Voltage dropped symmetrically across a plane cannot drive a cable mounted to the center of a board.

rotated 360°. The maximum radiation was recorded by the spectrum analyzer. The resolution bandwidth and video bandwidth of the spectrum analyzer were 100 kHz.

B. Measurement Results

Fig. 10 compares the measured radiation from the board without load capacitors with the estimated maximum radiation calculated using the voltage-driven radiation algorithm, the current-driven CM radiation algorithm, and the power bus radiation algorithm. The algorithm results provide an effective upper bound on the radiated emissions at all evaluated frequencies.

The algorithms indicate that voltage-driven CM radiation must be the source of the first three emission peaks. Voltage-driven CM radiation and power bus radiation are independent of the location where the cable connects to the board. However, maximum current-driven CM radiation is only achieved when the cable connections are near the edge of the board, since the voltage dropped across the return plane $V_{\rm ret}$ is incapable of driving current onto a cable attached to the center of the board, as illustrated in Fig. 11.

Fig. 12 shows that the radiation from the unloaded board does not change significantly when the cable connection is moved from the center to the edge of the board (from connector position

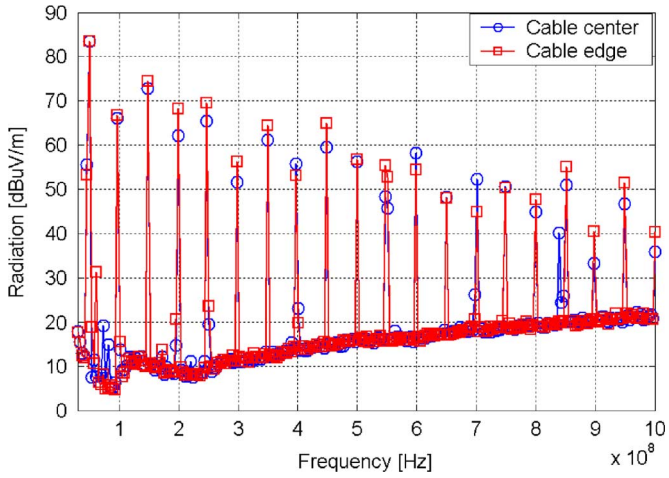

Fig. 12. Radiation from the board with cable position varied when the buffers were not loaded.

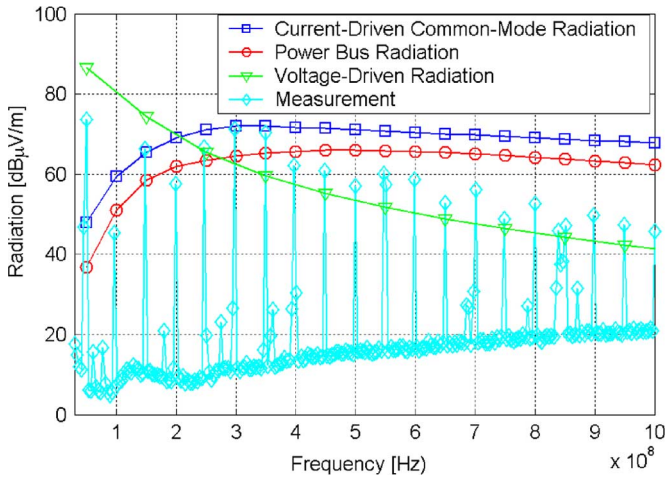

Fig. 13. Comparison of measured radiation and expert system algorithms calculation when the buffers were loaded with 1-nF capacitors.

1 to connector position 2 as shown in Fig. 2). This indicates that current-driven emissions are not a factor and is consistent with the algorithm prediction that the radiation is primarily voltage driven. Fig. 13 compares the measured radiation from the loaded board with the cable connection at the edge to the estimated maximum radiation calculated by the algorithms. Again, the expert system algorithm calculations provide an effective upper bound for the measured radiation. In this case, the algorithms indicate that the harmonics at 350 and 400 MHz are due to a current-driven source. They also suggest that the upper harmonic emissions are current driven, since they are higher when the outputs are loaded.

The cable connection was moved from the edge to the center of the board in order to eliminate current-driven emissions. Fig. 14 shows the measured emissions for both cable positions. Moving the cable to the center of the board reduced the emissions by 5–10 dB at the higher harmonics, confirming that the current-driven CM currents were primarily responsible for the radiated emissions above a few hundred megahertz.

It should be noted that the calculated radiation from the current-driven CM radiation algorithm and the power bus

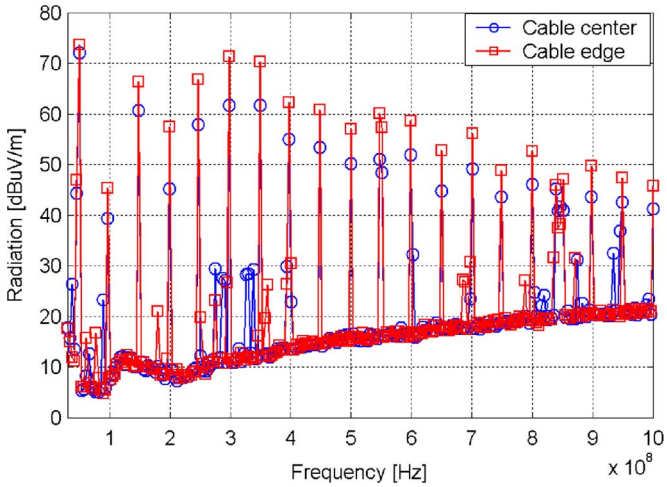

Fig. 14. Radiation from the board with cable position varied when the buffers were loaded with 1-nF capacitors.

radiation algorithm overestimate the radiation by about 10 dB at frequencies above 400 MHz. This is due to the triangular waveform used by these algorithms to represent the signal current. In situations where better accuracy at high frequencies is required, the triangular waveforms in Fig. 6 can be replaced by double exponential waveforms, as described in [19].

V. Conclusion

The radiation from a test board was estimated using three EMI radiation algorithms developed for PCB EMC expert system software. The calculated maximum radiation from the board in two cases, where the buffers on the board were not loaded or loaded with 1-nF capacitors, was compared to measurement results. Both the calculations and measurements show that the voltage-driven radiation mechanism dominates over most of the frequency range evaluated when the buffers are not loaded. They also show that the current-driven CM radiation mechanism dominates at high frequencies when the buffers are loaded with 1-nF capacitors. In both cases, the algorithms provided an effective upper bound estimate for the radiated emissions.

Of course, the goal of expert system algorithms is not to predict radiated emissions but rather to identify the structures capable of creating a radiated emissions problem. The results presented here indicate that the algorithms were capable of identifying the primary source structures and coupling mechanisms for the test board evaluated.

References

[1] K. Nageswara Rao, P. Venkata Ramana, M. V. Krishnamurthy, and K. Zinnias, "EMC analysis in PCB designs using an expert system," in *Proc. Electromagn. Interference Compat., Int. Conf.*, Madras, India, Dec. 1995, pp. 59–62.

[2] T. Hubing, J. Drewniak, T. Van Doren, and N. Kashyap, "An expert system approach to EMC modeling," in *Proc. IEEE Int. Symp. Electromagn. Compat.,* Aug. 19–23, 1996, pp. 200–203.

[3] N. Kashyap, T. Hubing, J. Drewniak, and T. Van Doren, "An expert system for predicting radiated EMI from PCB's," in *Proc. IEEE Int. Symp. Electromagn. Compat.,* Aug. 18–22, 1997, pp. 444–449.

[4] A. Drozd, A. Pesta, D. Wiener, P. Varshney, and I. Demirkiran, "Application and demonstration of a knowledge-based approach to interference rejection for EMC," in *Proc. IEEE Int. Symp. Electromagn. Compat.,* Aug. 24–28, 1998, vol. 1, pp. 537–542.

[5] Demirkiran, V. N. S. Samarasooriva, P. K. Varshney, D. D. Weiner, R. Mani, S. Hamid Nawab, and S. Tyler, "Knowledge-based approach to interference rejection for EMC," in *Proc. IEEE Int. Symp. Electromagn. Compat.,* Aug. 24–28, 1998, vol. 2, pp. 1150–1155.

[6] S. Ranganathan, D. Beetner, R. Wiese, and T. Hubing, "An expert system architecture to detect system-level automotive EMC problems," in *Proc. IEEE Int. Symp. Electromagn. Compat.*, Minneapolis, MN, Aug. 2002, pp. 976–981.

[7] H. Shim, T. Hubing, T. Van Doren, R. DuBroff, J. Drewniak, D. Pommerenke, and R. Kaires, "Expert system algorithms for identifying radiated emission problems in printed circuit boards," in *Proc. IEEE Int. Symp. Electromagn. Compat.*, Santa Clara, CA, vol. 1, Aug. 9–13, 2004, pp. 57–62.

[8] H. Shim and T. Hubing, "Model for estimating radiated emissions from a printed circuit board with attached cables driven by voltage-driven sources," *IEEE Trans. Electromagn. Compat.*, vol. 47, no. 4, pp. 899–907, Nov. 2005.

[9] H. Shim and T. Hubing, "Derivation of a closed-form approximate expression for the self-capacitance of a printed circuit board trace," *IEEE Trans. Electromagn. Compat.*, vol. 47, no. 4, pp. 1004–1008, Nov. 2005.

[10] D. Hockanson, J. Drewniak, T. Hubing, F. Sha, and M. Wilhelm, "Investigation of fundamental EMI source mechanisms driving common-mode radiation from printed circuit boards with attached cables," *IEEE Trans. Electromagn. Compat.*, vol. 38, no. 4, pp. 557–565, Nov. 1996.

[11] H. Shim, Y. Fu, and T. H. Hubing, "Radiated emissions from populated printed circuit boards due to power bus noise," in *Proc. IEEE Int. Symp. Electromagn. Compat.*, Santa Clara, CA, vol. 2, Aug. 9–13, 2004, pp. 396–400.

[12] H. Shim and T. Hubing, "A closed-form expression for estimating radiated emissions from the power planes in a populated printed circuit board," *IEEE Trans. Electromagn. Compat.*, vol. 48, no. 1, pp. 74–81, Feb. 2006.

[13] National Center for Manufacturing Sciences, "Embedded decoupling capacitance project final report," NCMS Rep. 0091RE00, Dec. 2000.

[14] A. R. Scott, "Simulation tools for the analysis of single electronic systems" Ph.D. dissertation, Dept. Electron. Electr. Eng., Univ. Glasgow, Glasgow, U.K., 1994.

[15] K. C. Gupta, R. Garg, and I. Bahl, *Microstrip Lines and Slot Lines*, 2nd ed. Norwood, MA: Artech House, 1996.

[16] F. Schnieder and W. Heinrich, "Model of thin-film microstrip line for circuit design," *IEEE Trans. Microw. Theory Tech.*, vol. 49, no. 1, pp. 104–110, Jan. 2001.

[17] M. Leone, "The radiation of a rectangular power-bus structure at multiple cavity-mode resonances," *IEEE Trans. Electromagn. Compat.*, vol. 45, no. 3, pp. 486–492, Aug. 2003.

[18] J. Fan, W. Cui, J. L. Drewniak, T. P. Van Doren, and J. L. Knighten, "Estimating the noise mitigation effect of local decoupling in printed circuit boards," *IEEE Trans. Adv. Packag.*, vol. 25, no. 2, pp. 154–165, May 2002.

[19] Y. Fu, G. L. Burbui, and T. Hubing, "An improved model for representing current waveforms in CMOS circuits," Clemson Veh. Electron. Lab., Clemson, SC, Tech. Rep. CVEL-06-01, Sep. 2006.

Yan Fu received the B.S. degree in electrical and mechanical engineering from the Beijing Institute of Technology, Beijing, China, and the M.S. degree in electrical engineering from the University of Missouri-Rolla in 1996 and 2004, respectively.

From 2003 to 2005, she was a Graduate Research Assistant in the Electromagnetic Compatibility Laboratory, University of Missouri-Rolla. Her research interests include signal integrity and electromagnetic compatibility.

Todd Hubing (S'82–M'82–SM'93–F'96) received the B.S.E.E. degree from the Massachusetts Institute of Technology, Cambridge, in 1980, the M.S.E.E. degree from Purdue University, West Lafayette, IN, in 1982, and the Ph.D. degree in electrical engineering from North Carolina State University, Raleigh, in 1988.

From 1982 to 1989, he was in the Electromagnetic Compatibility Laboratory, IBM Communications Products Division, Research Triangle Park, NC. In 1989, he joined the University of Missouri-Rolla (UMR) as a Faculty Member. Since 2006, he has been with Clemson University, Clemson, SC, as the Michelin Professor for Vehicular Electronics. His current research interests include electromagnetic compatibility and computational electromagnetic modeling, as applied to automotive and aerospace electronic designs, in particular.

Prof. Hubing was an Associate Editor of the IEEE TRANSACTIONS ON ELECTROMAGNETIC COMPATIBILITY, the IEEE ELECTROMAGNETIC COMPATIBILITY SOCIETY NEWSLETTER, and the *Journal of the Applied Computational Electromagnetics Society*. He was on the Board of Directors for the Applied Computational Electromagnetics (EMC) Society and the IEEE Electromagnetic Compatibility Society. He was the President of the IEEE EMC Society from 2002 to 2003.